Q. J. R. Meteorol. Soc. (1996), **122**, pp. 1385–1404

Monsoons and the dynamics of deserts

By MARK J. RODWELL* and BRIAN J. HOSKINS
University of Reading, UK

(Received 12 April 1995; revised 21 December 1995)

SUMMARY

The existence of subtropical deserts, such as the Sahara, has often been attributed to the annual-mean, zonal-mean Hadley circulation which shows strong descent in the subtropics. However, the zonal-mean Hadley circulation shows considerable evolution over the course of the year with very strong subtropical descent during winter, but practically no zonal-mean subtropical descent during summer when rainfall over the eastern Sahara and the Mediterranean is least. Charney (1975) proposed a biosphere–albedo feedback mechanism whereby local anthropogenic effects related to over-grazing could affect the radiative balance, enhancing summertime *diabatic* descent and leading to desertification of the subtropics in general. The present study, which uses an idealized model, suggests a monsoon–desert mechanism for desertification whereby remote diabatic heating in the Asian monsoon region can induce a Rossby-wave pattern to the west. Integral with the Rossby-wave solution is a warm thermal structure that interacts with air on the southern flank of the mid-latitude westerlies causing it to descend. This *adiabatic* descent is localized over the eastern Sahara and Mediterranean, and over the Kyzylkum desert to the south-east of the Aral Sea, by the mountains of north Africa and south-west Asia. Trajectories indicate that the monsoon–desert mechanism does not represent a simple 'Walker-type' overturning cell. Instead, the descending air is seen to be mainly of mid-latitude origin. It is speculated that the monsoon-forced adiabatic descent may result in clear air and, therefore, a local diabatic enhancement which effectively doubles the strength of descent. With this mechanism, desertification can be forced by *remote* changes in monsoon strength rather than by *local* effects. This conclusion is supported by the observed dramatic strengthening of descent over the Mediterranean and east Sahara during the onset of the Asian monsoon and, on the longer timescale, by relating prehistoric lake-levels to Milankovitch–monsoon forcing. The latter may help to explain the perceived discrepancies between the palaeoclimate of the eastern Sahara and the strength of a 'tropic-wide' monsoon. The monsoon–desert mechanism may not be confined to the Asian monsoon alone and the existence of other monsoon-climate regions over the globe may, in a similar way, explain the observed summertime strengthening of the oceanic sub-tropical anticyclones and the existence of western continental deserts and 'Mediterranean-type' climate regions.

KEYWORDS: Desertification Monsoon flow Paleolakes Rossby waves Sahara

1. INTRODUCTION

The existence of subtropical deserts is often attributed to the descending branch of the zonal-mean tropical Hadley circulation. With a lack of moist convective heating, radiative cooling is balanced by adiabatic warming associated with the descent:

$$\frac{Q}{c_p} = \left(\frac{p}{p_0}\right)^{\kappa} \omega \frac{\partial \theta}{\partial p}, \tag{1}$$

with the usual notation as given in the appendix. Charney (1975) highlighted the observation that desert regions are areas of net radiative heat loss, and that since the compensating descent decreases the relative humidity, 'the desert enhances its own dryness'.

Charney (1975) proceeded to propose a biosphere–albedo feedback mechanism that could enhance the effects of the mean Hadley circulation and account for desert growth. In this model, the increase in albedo associated with an *imposed* reduction in vegetation cover, $-\delta A_i$, leads to enhanced radiative cooling. This in turn is balanced by enhanced descent, reduced rainfall and a consequent decrease in the *potential* vegetation cover that can be sustained, $-\delta A_p$. For Charney's model to give instability it is necessary that $\delta A_p > \delta A_i$. Nevertheless, even if this inequality does not hold, there is the possibility of a large response to anthropogenic forcing.

Subsequent comments by Ripley (1976), Ellsaesser *et al.* (1976) and Idso (1977) noted the possible importance of latent-heat fluxes over vegetated areas which were ignored in

* Corresponding author: University of Reading, Department of Meteorology, 2 Earley Gate, Whiteknights, PO Box 239, Reading, Berkshire RG6 6AU, UK.

Charney's theoretical model. However, GCM modelling results of both Charney (1975), and Ellsaesser *et al.* (1976), tended to support the idea that increased albedo was associated with reduced precipitation.

On closer inspection, there is no doubt that a simple zonal-mean Hadley-cell argument for the existence of deserts does not work. The zonal-mean Hadley circulation has its descending branch over the northern subtropics between December and February, whereas there is very little zonal-mean vertical motion at 25°N during the June–August season when parts of North Africa and the Mediterranean are at their driest. Latitude 25°N includes the Sahara Desert but also the Asian summer monsoon (Cherrapunji with 11 m of rain per year is one of the wettest places on Earth) and the Florida Everglades; the question arises as to the influence of monsoons, and in particular the Asian summer monsoon, on the summertime descent over subtropical desert regions.

In the idealized Asian summer-monsoon simulation of Gill (1980), a region of weak Rossby-wave descent can be seen to the west of the imposed heating, a similar configuration to that of the Sahara/Mediterranean and the real Asian summer monsoon. Gill's model, which follows closely the lines of Matsuno (1966), is linearized about a resting atmosphere and the underlying thermodynamic equation may be written as an extension of (1):

$$\frac{Q}{c_p} = \left(\frac{p}{p_0}\right)^{\kappa} \omega \frac{\partial \theta}{\partial p} + \varepsilon T', \tag{2}$$

where T' is the temperature perturbation and ε is a damping coefficient. The compensating descent in the absence of any other diabatic forcing, $Q = 0$, depends critically on the damping timescale, ε^{-1}. In his paper, Gill used a relatively large damping with a timescale of about two days. A more realistic timescale would probably be significantly longer.

The aim of the present paper is to demonstrate that the Asian summer monsoon does indeed generate significant descent to its west. This descent can be associated with the Rossby-wave response to the heating but the simple thermodynamic budgets (1) and (2) do not describe the relevant balance.

Figure 1(a) shows the 'observed' June to August vertical velocity, $\omega = \mathrm{D}p/\mathrm{D}t$, at 477 hPa which has been spectrally smoothed, following Hoskins (1980), using a scale-selective filter that involves multiplying a spectral coefficient whose total wave-number is n by $\exp[-K\{n(n+1)\}^2]$. K is chosen so that this factor is 0.1 for $n = 24$. Ascent, centred over the north Bay of Bengal, is clearly shown in the Asian monsoon region. Ascent is also seen in the intertropical convergence zone (ITCZ) over equatorial Africa. To the west of the Asian monsoon region, between about 30°N and 40°N, there are clear centres of strong and localized summertime descent. The eastern-most centre, at about 60°E, 40°N, is located over the Kyzylkum desert region, south-east of the Aral Sea. The strongest descent is centred over the eastern Mediterranean, covering south-eastern Europe and the eastern Sahara Desert. A third centre, associated with the North Atlantic sub-tropical anticyclone, occurs over the east Atlantic at the same latitude. Various descent centres are seen south of the equator in the longitudinally-extended descending branch of the tropical Hadley circulation. Wherever time-mean descent exists, it is likely to inhibit convection and would be consistent with dry or arid conditions.

The nature of the thermodynamic budget in the region of *ascent* is relatively simple. Figure 1(b, d) shows that the thermodynamic energy balance at 477 hPa is quite precisely given by (1). Latent-heat release from deep convection in the ITCZ and the Asian monsoon region (Fig. 1(b)) is balanced almost entirely by adiabatic cooling due to ascent (Fig. 1(d)).

Charney (1975), amongst others, assumed that the same balance operated over the desert regions. However the evidence from the budget terms shown in Fig. 1 is that the

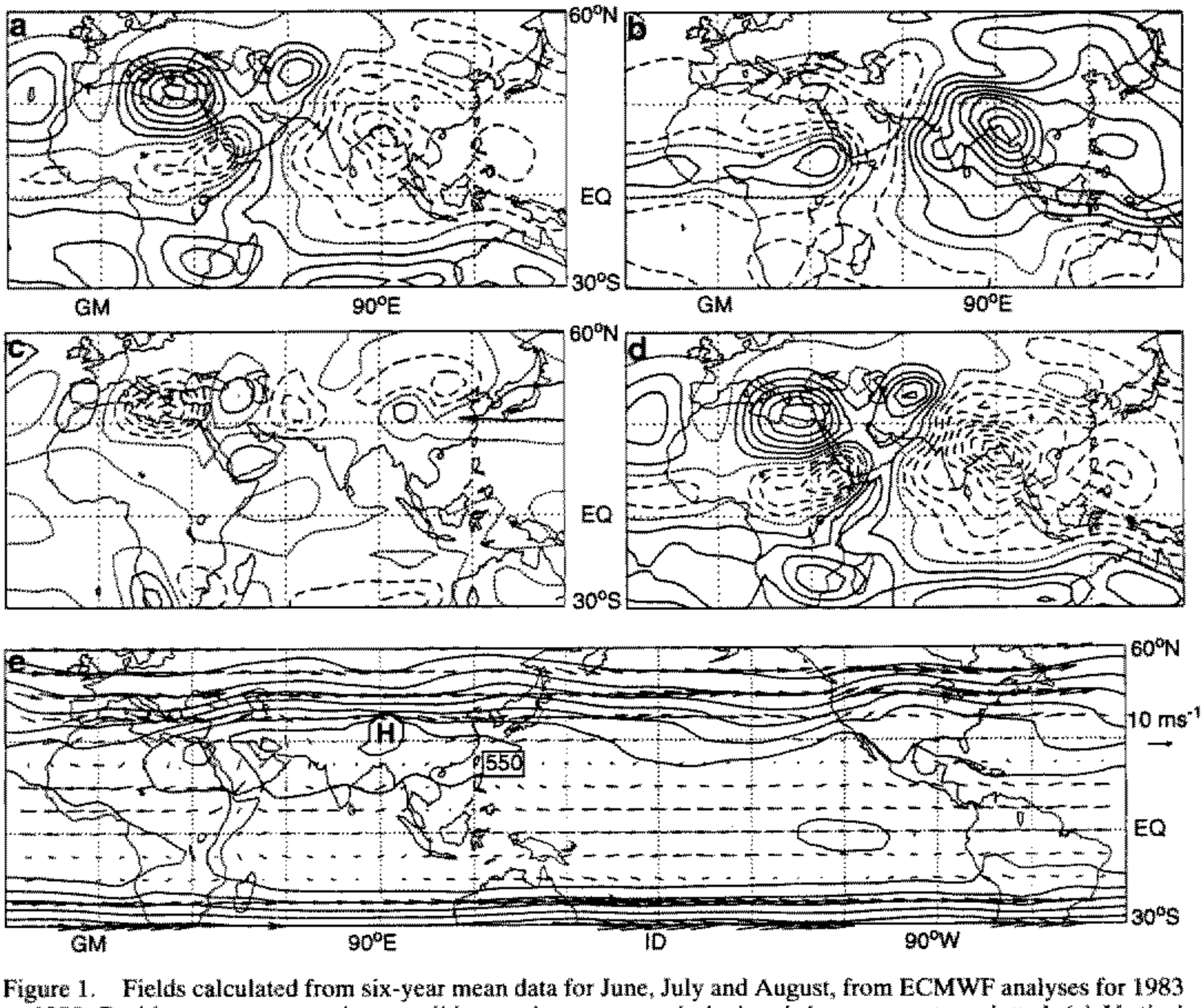

Figure 1. Fields calculated from six-year mean data for June, July and August, from ECMWF analyses for 1983 to 1988. Positive contours are shown solid, negative contours dashed and the zero contour dotted. (a) Vertical velocity, ω, at 477 hPa with contour interval 0.5 hPa h^{-1}. (b), (c) and (d) show terms in the thermodynamic-energy equation calculated at 477 hPa with contour interval 0.5 K day^{-1}: (b) diabatic heating, Q/c_p; (c) horizontal advection, $-\mathbf{V} \cdot \nabla_p T$, and (d) vertical advection, $-(p/p_0)^\kappa \omega \partial\theta/\partial p$. (e) Pressure and horizontal winds on the 325 K isentropic surface with contour interval 40 hPa and 'H' indicating pressure higher than 590 hPa.

balance is more complicated, with the horizontal advection term, Fig. 1(c), showing a strong contribution. In general, in these northern hemisphere descent regions, the time-mean horizontal-advection term is perhaps twice as strong as the time-mean diabatic-cooling term and the thermodynamic-energy equation must include this horizontal advection;

$$\frac{Q}{c_p} = \mathbf{v} \cdot \nabla_p T + \left(\frac{p}{p_0}\right)^\kappa \omega \frac{\partial \theta}{\partial p}. \tag{3}$$

Moreover, the positioning of the descent regions, seen in Fig. 1(a) is more closely aligned to the structure of the horizontal advection term, Fig. 1(c), than to the structure of the diabatic term, Fig. 1(b). It appears that the horizontal-advection term, far from being negligible, could well be central to the location and existence of these desert regions.

The suspected importance of the horizontal-advection term is not incompatible with the thermodynamic-energy budgets calculated by Bounoua and Krishnamurti (1991) who investigated the desert heat-low mechanism and indicated that, at this level, horizontal advection was small. Their region of interest (10°W to 20°E and 15°N to 30°N) was considerably different from the present east Saharan 'descent region' and, indeed, an area average of the horizontal-advection term in Fig. 1(c) over their region of interest would

show very little signature. Clearly, the desert heat-low mechanism is a vital aspect of the local desert circulation but, being a local mechanism and dependent on the prior existence of arid conditions, it cannot explain the localization and initiation of sub-tropical deserts—the question of interest here.

The discussion here is consistent with that given by Hoskins (1986) who produced a scaling analysis for the large-scale thermodynamic equation. The balance of terms was related to the Burger number, $B = N^2H^2/f^2L^2$. In the equatorial region B is large which implies that horizontal advection is negligible compared with vertical advection, so that the balance is between this adiabatic warming and cooling associated with vertical motion on the one hand, and diabatic effects on the other. In the large-scale equivalent-barotropic stationary waves in the middle latitudes, B is small so that, to a first approximation, horizontal advection balances diabatic heating. This is the 'advective limit' of Smagorinsky (1953). However, in the large-scale motion in the subtropics, B is of order unity so that both horizontal and vertical advection must be included.

In a hypothetical adiabatic situation with diabatic heating and cooling ignored, suggested above as a first approximation for the *descent regions* by the horizontal structures of the terms in (3), air will remain on isentropic surfaces. Figure 1(e) shows the observed pressure and horizontal winds on the 325 K isentropic surface. The H printed near 90°E, 30°N represents a high-pressure centre, with pressure in excess of 590 hPa. The 325 K isentropic surface intersects the Tibetan Plateau in this region, which is why contours bunch immediately to the north. In the hypothetical steady-adiabatic situation, cross-contour flow in Fig. 1(e) indicates vertical motion, ω. In both the desert-descent regions, the 'westerly' flow has a northerly component, giving cross-contour flow and descent. Importantly, there is also a west to east gradient of pressure on the isentropic surface so that, in addition, the *westerly* winds give cross-contour flow and descent.

Figure 1(e) can be inverted and thought of as temperature, T, on a pressure surface. For small amplitude variations and uniform $\partial\theta/\partial p$, this inversion is quantitatively correct. The Asian monsoon region is then seen as a significant 'hot-spot' in the zonal-mean temperature. When viewed in this way, cross-contour flow in Fig. 1(e) represents the regions of horizontal temperature-advection, seen in Fig. 1(c). This adiabatic scenario is used in the present study as a starting point for the investigation into a desert mechanism.

In section 2, a brief outline of the full model and data used for this study are given, together with two preliminary simulations which are used to show the performance of the model and to justify the more idealized model integrations presented in section 3. In section 3, results from idealized integrations suggest a monsoon–desert mechanism that helps to explain, for example, the existence and location of the Sahara, the Mediterranean-type climate and perhaps even the drying-up of the Aral Sea. In section 4, other evidence for the monsoon–desert mechanism on seasonal and Milankovitch timescales is presented. A discussion is given in section 5.

2. Model and data

The model used in this investigation has been explained in detail by Hoskins and Rodwell (1995). It is a time-dependent, global, hydrostatic, primitive-equation model derived from Hoskins and Simmons (1975). It is nonlinear, spectral in the horizontal and uses finite differences in σ-coordinates in the vertical. The horizontal resolution is triangular truncation 31 and there are 15 levels in the vertical. The model is initiated with the zonal mean of a six-year June to August climatology derived from initialized analyses from the European Centre for Medium-Range Weather Forecasts (ECMWF) for 1983 to 1988 (Hoskins *et al.* (1989)). A smoothed earth orography, shown in Fig. 2(a), is raised over

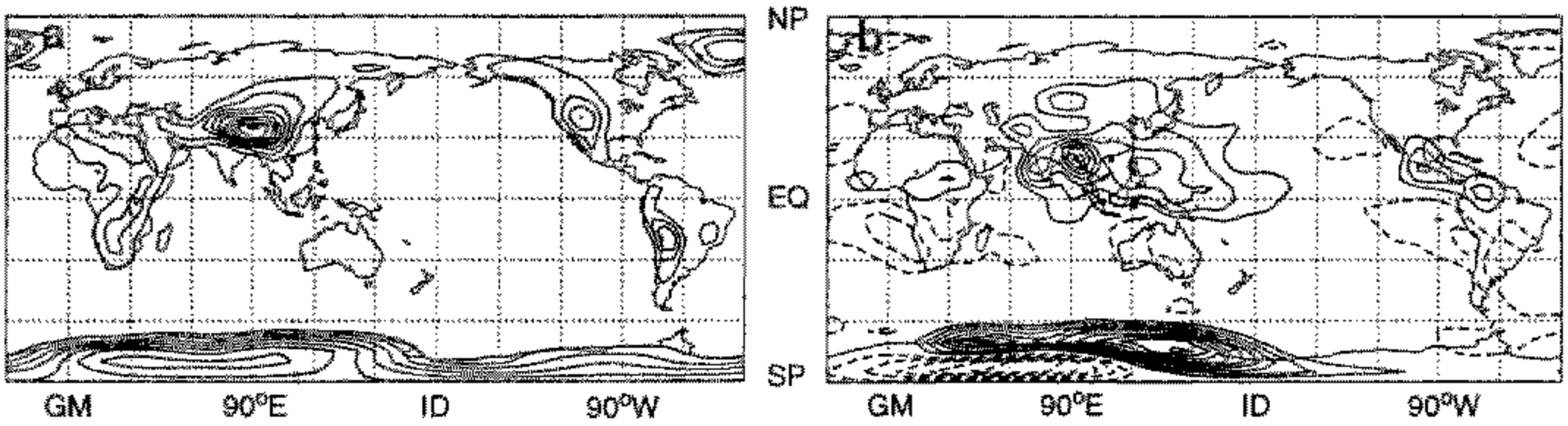

Figure 2. (a) Global orography derived from 1° × 1° data and spectrally smoothed. The contour interval is 500 m. (b) Column mean of the 6 year (1983 to 1988) June, July and August diabatic-heating field calculated from ECMWF analyses as a residual in the time-mean thermodynamic-energy equation. The contour interval is 50 W m^{-2}. In both panels, positive contours are solid, negative contours are dashed and the zero contour has been suppressed.

the first five days of an integration and hydrostatic adjustments are made to the temperature and surface pressure so that a near steady-state solution to topography is achieved as quickly as possible. At day 5, the global diabatic-heating field, calculated as a residual in the time-mean thermodynamic-energy equation using the six-year mean data, is applied as a constant forcing. Although the model does not include moisture explicitly, this forcing mimics, in a non-interactive way, the effects of, for example, latent-heat release and radiation budgets. Figure 2(b) shows the column mean of this field. The model uses a simple linear drag in the lowest two levels, $\sigma = 0.887, 0.967$, on timescales of 5 days and 1 day, respectively, over the oceans, and 5/4 and 1/4 days, respectively, over land areas. Newtonian cooling towards the basic state (with the same adjustments for orography) is applied with a timescale of 25 days over much of the atmosphere, but decreasing to 5 days in the boundary layer to simulate surface effects. A ∇^6 horizontal hyperdiffusion, with a timescale of six hours on the smallest retained horizontal scale, is applied to the vorticity, divergence and temperature. With the exception of the hydrostatic adjustments to the changing orography, the zonal averages of vorticity, divergence, temperature and surface pressure are held constant throughout the integration.

Initially, after turning on the heating, the modelled circulation evolves rapidly. The low-level westerly winds over India, for example, seen in Fig. 3(a), increase in an explosive fashion (Fig. 3(c) solid curve), somewhat like the real monsoon onset. Some five days later, the flow pattern becomes more steady and, importantly, very similar to the 'observed' June to August mean flow. The horizontal line in Fig. 3(c) indicates the mean observed value for the index of about 9.3 m s^{-1}. The similarity is important because the moisture fluxes that would be inferred from the model's circulation are then consistent with the latent-heat release imposed on the diabatic term. This helps justify the prescription of the fixed diabatic forcing in the first place.

It should be mentioned that, over the Sahara, and the tropics and subtropics in general, observations are rather sparse so that, for the analysis at a particular time, the ECMWF model's earlier forecast for that time plays an important role. With this proviso always in mind, the six-year June to August climatology derived from initialized analyses from ECMWF for 1983 to 1988 is referred to here as the 'observed' circulation.

Later on in the simulation, from perhaps day 20, mid-latitude baroclinic instability begins to influence the simulation and, because of the simplicity of the model, it does so in an unrealistic manner. However, for the purposes of the present investigation, which is concerned with the direct effects of tropical heating, this is not important. Results are generally shown for a time when the flow is nearly steady, after the model has adjusted to the imposed heating and before baroclinic instability sets in.

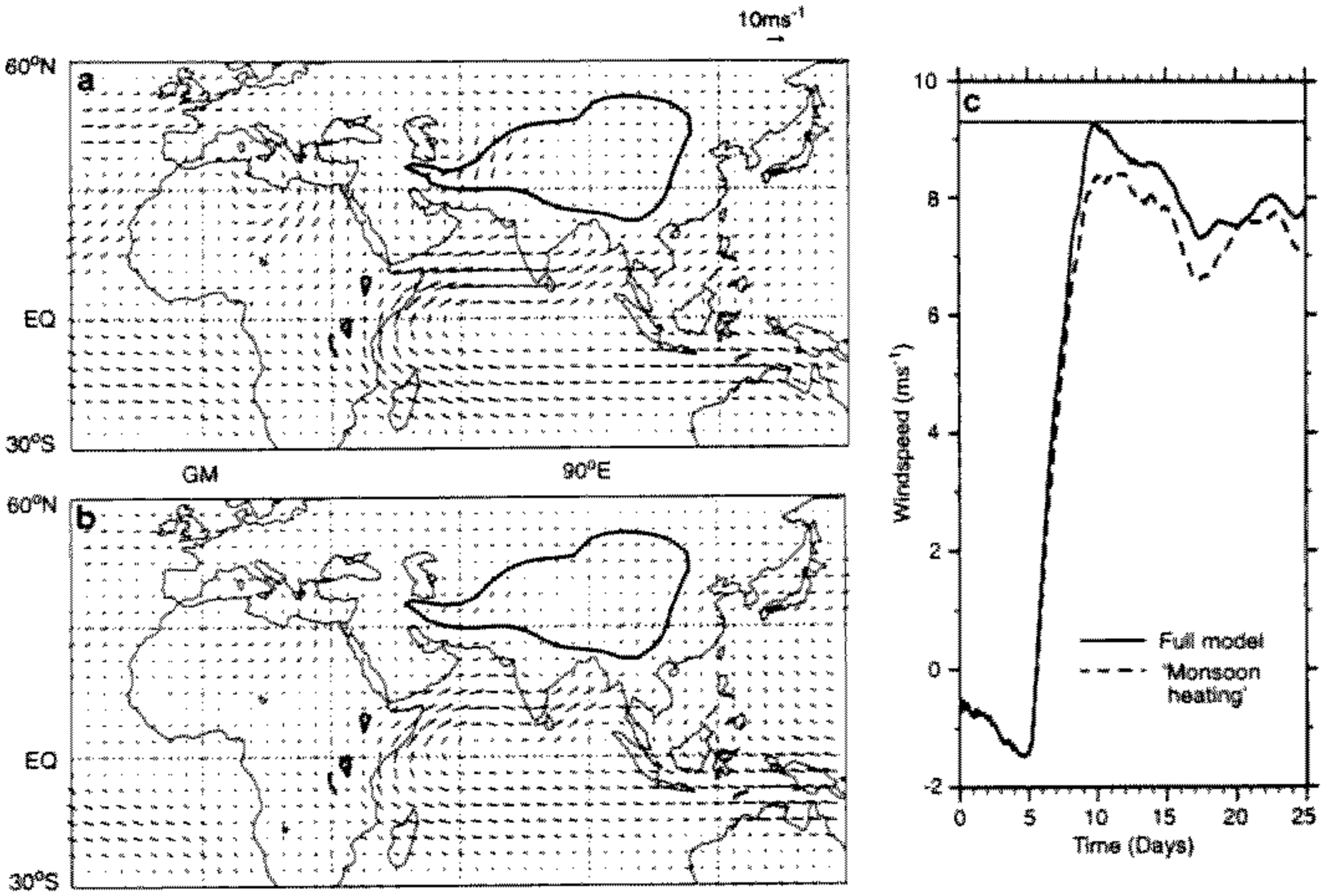

Figure 3. (a) and (b) Low-level wind vectors at 887 hPa for day 16 of two model integrations: (a) the full model, (b) an integration where diabatic heating is only applied in the 'monsoon region' (60°–150°E and 10°–60°N). The solid contours show where this isobaric surface intersects the model's orography and the interpolated wind vectors within this line should be ignored. (c) Strength of the 887 hPa westerly flow in a box covering southern India (75° to 90°E and 9.3° to 16.7°N). The solid curve is for the full model integration; the dashed curve is for the monsoon heating integration. The horizontal line shows the time-mean observed westerly wind speed.

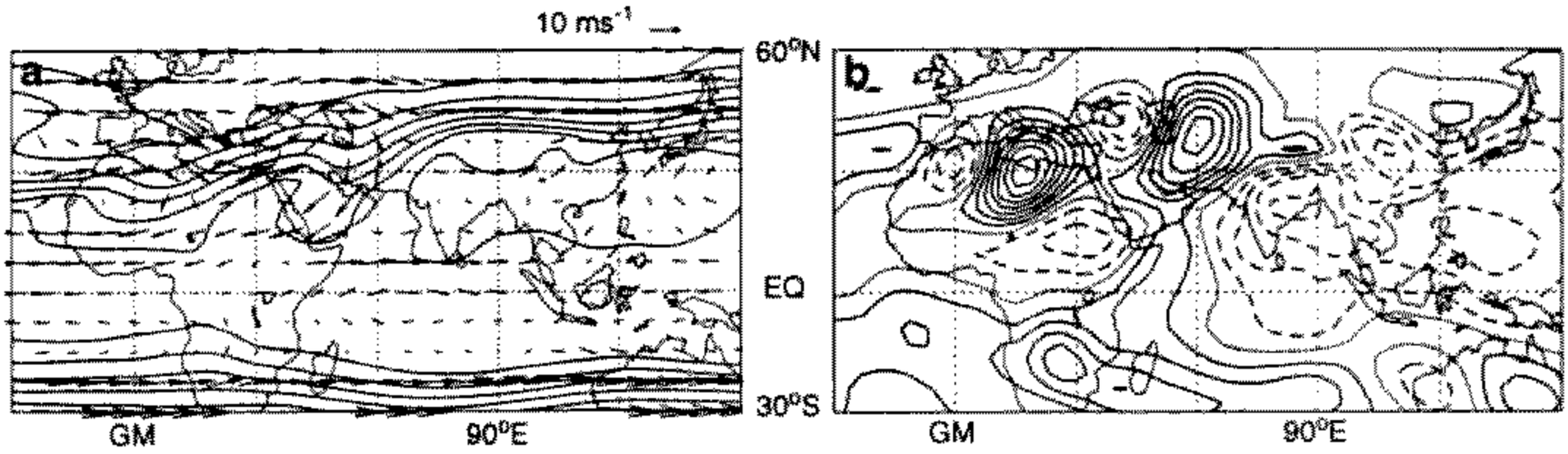

Figure 4. (a) Pressure and horizontal winds on the 325 K isentropic surface for day 16 of the standard model integration; the contour interval is 40 hPa. (b) Vertical velocity, ω, on 477 hPa for day 16 of the standard integration; the contour interval is 0.5 hPa hr^{-1}.

Figure 4(a) shows the day 16 pressure and horizontal winds on the 325 K isentropic surface for the standard integration, outlined in section 2. The monsoon 'hot-spot' is simulated, as are the anticyclonic centres and the cross-contour flow. The northerly flow in the Aral Sea centre is too intense and appears to advect more cold air from the north over the Arabian Peninsula, splitting the monsoon warm region.

Figure 4(b) shows vertical velocity at 477 hPa at day 16 of the full model integration. Both desert descent regions are well located, the Saharan one being of the correct intensity whilst, consistent with the enhanced magnitude of the horizontal thermal-advection, the centre near the Aral Sea is too intense. A possible reason for the exaggerated Aral Sea

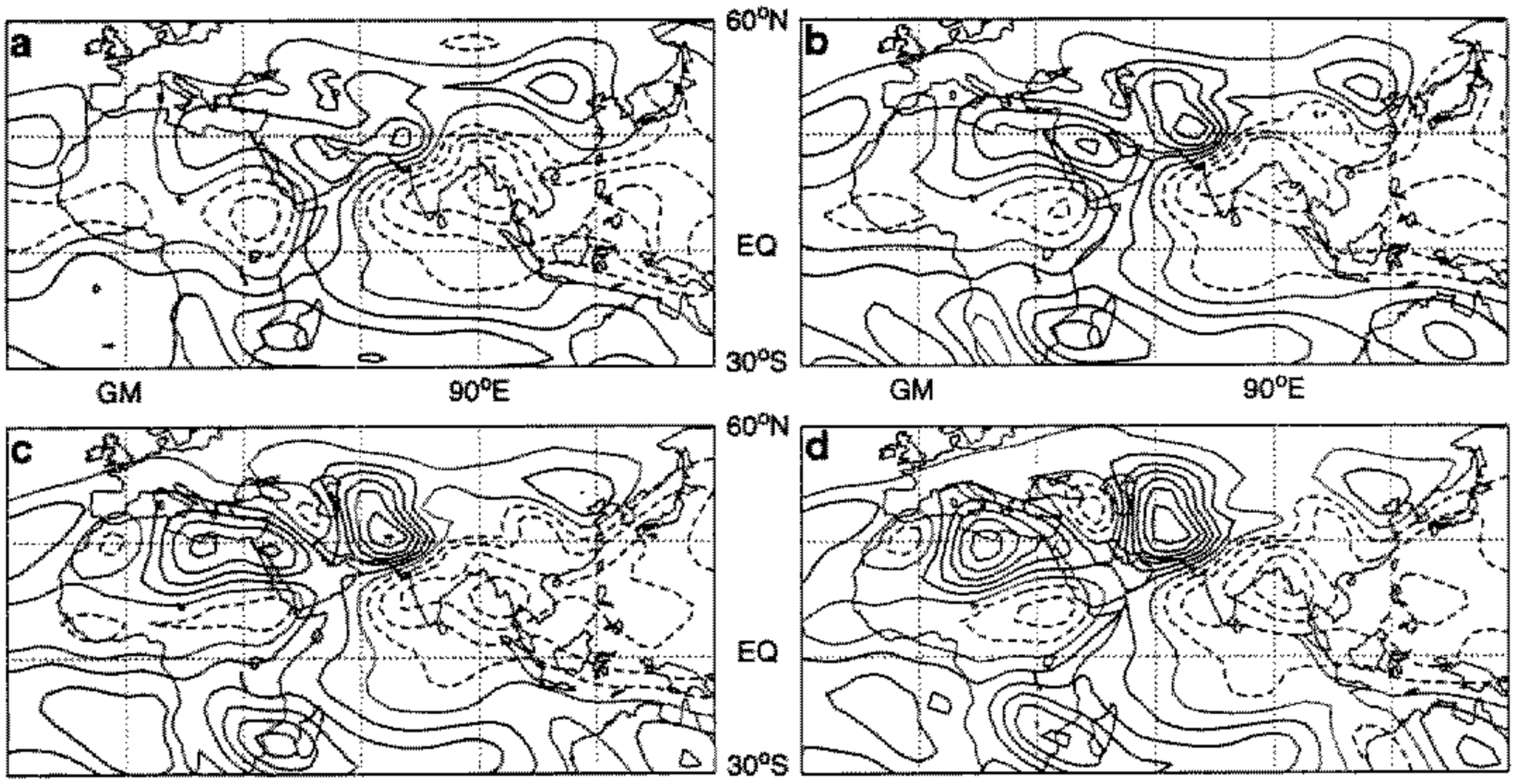

Figure 5. Vertical velocity, ω, on 477 hPa for the standard integration: (a) day 7; (b) day 9; (c) day 11; (d) day 13. The contour interval is 0.5 hPa hr^{-1}.

descent is given later. With the exception of this increased horizontal-advection centre over the Aral Sea region, the modelled thermodynamic balance is found to be very similar to the 'observed' one shown in Fig. 1.

Figure 5 shows the development of the modelled descent. At day 7, Fig. 5(a), two days after the diabatic forcing was turned on, the areas of descent over north Africa, the Mediterranean, and the Arabian Peninsula coincide with the diabatic cooling at this level shown in Fig. 1(b). On day 9, Fig. 5(b), descent over the Arabian Peninsula is particularly strong. Over the next few days (days 11 and 13 are given in Fig. 5(c, d) and day 16 in Fig. 4(b)) the north African centre strengthens and the Arabian Peninsula centre weakens. The effect appears to be a westward movement of the region of maximum descent away from the monsoon region, and timescales for this movement agree well with the Rossby-wave propagation of Heckley and Gill (1984). However, the geographically-fixed forcing of the mountains and the *local* prescribed diabatic cooling tend to obscure the pure response to *remote* monsoon forcing.

Before investigating the effect of the monsoon on the deserts to its west, it is perhaps worth first demonstrating that these deserts do not themselves appear to have a great influence on the mean monsoon. Figure 3(b) shows the low-level circulation at day 16 of a model simulation where the diabatic forcing has been applied only in the 'monsoon region' (60°E to 150°E and 10°N to 60°N). The monsoon in-flow which is vital as a moisture source for the monsoon rains remains almost unaltered when compared with the full model simulation in Fig. 3(a) (or indeed to the observations given by Rodwell and Hoskins (1995)). Figure 3(c) shows that the strength of the low-level westerly flow over southern India is quantitatively little changed. Again, therefore, we argue that the *implied* moisture fluxes into the monsoon region are consistent with the *applied* diabatic forcing. Transients, including those possibly emanating from the desert regions, may, of course, affect the instantaneous monsoon; however, the above result is justification for the modelling approach taken here where we now apply more idealized monsoon heatings and apply zero heating above the desert regions. This approach was suggested above, based on the thermodynamic-energy equation balance.

3. The monsoon–desert mechanism

(*a*) *The remote monsoon effect*

To study the importance of the Indian monsoon in the formation of descent to its west and northwest, a series of integrations was made using a simple idealized elliptical 'monsoon' heating. Figure 6(a) shows the column mean of the heating when it is centred at 90°E, 10°N. This idealized heating is representative of deep convection with a maximum of 5 K day^{-1} at about 400 hPa. No orography is used in this series of integrations and so the heating is turned on at day zero. Consequently, day 11 corresponds to heating for the same length of time as day 16 of the standard integration.

The first integration of the series is a linear integration, linearized about a resting basic state, $\mathbf{v} = 0$, $\nabla_\sigma T = 0$. The linearization procedure has been explained by Hoskins and Rodwell (1995). The heating is centred at 10°N as in Fig. 6(a). There is no maintenance of the zonal mean of the (resting) basic state and drag and thermal damping are turned off. This integration represents about the closest the present model can be to the time-dependent model of Heckley and Gill (1984).

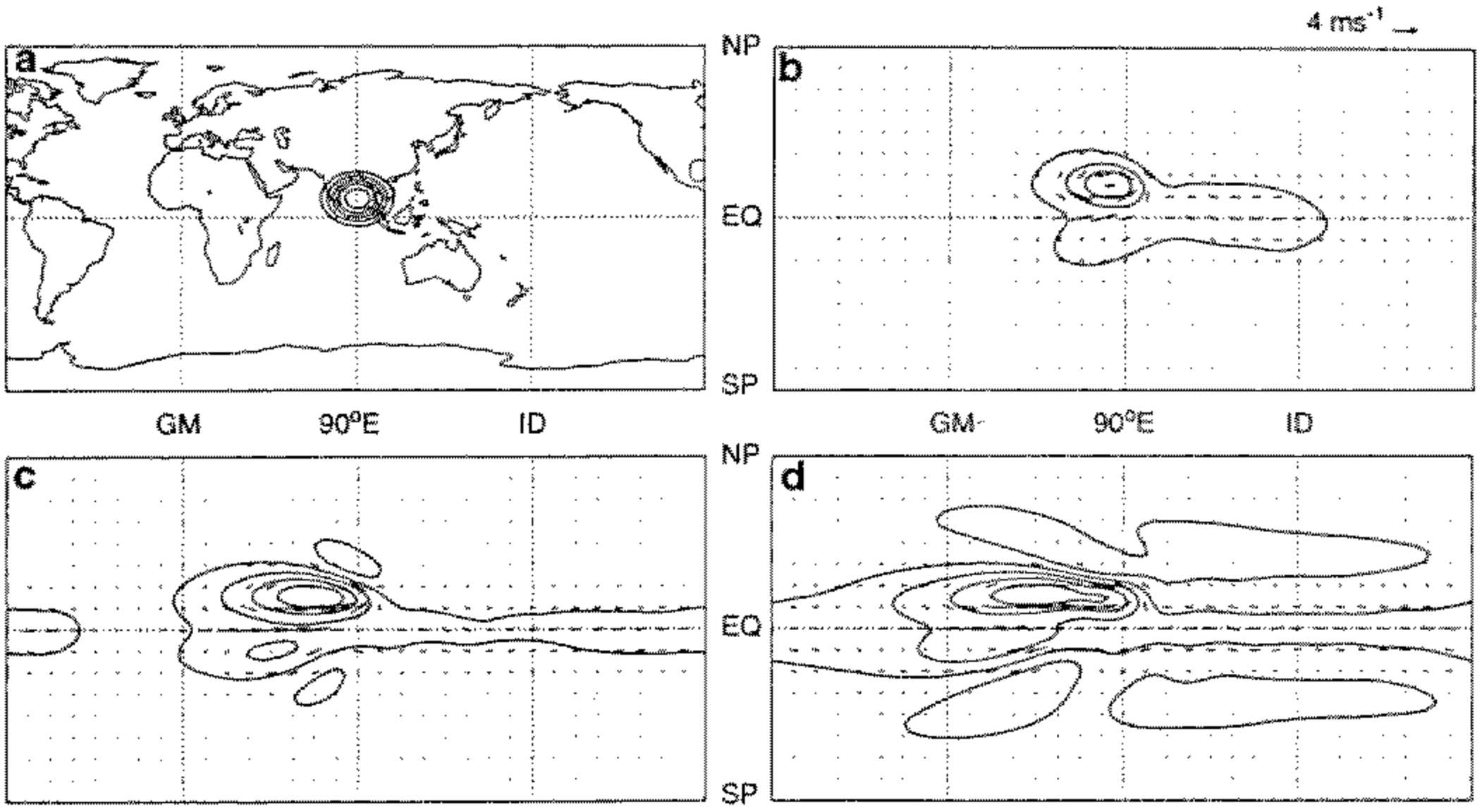

Figure 6. (a) Column-mean diabatic heating centred at 90°E, 10°N. The contour interval is 50 W m^{-2}; the zero contour is not shown. (b), (c) and (d) show the corresponding perturbation surface pressure and 887 hPa horizontal winds for an integration linearized about a resting basic-state at (b) day 3, (c) day 7 and (d) day 11. The contour interval is 1 hPa.

Figure 6(b, c, d) shows the modelled perturbation surface pressure and 887 hPa horizontal winds at days 3, 7 and 11. As in the case reported by Jin and Hoskins (1995), there is very good qualitative agreement with the analytical results of Gill (1980), Heckley and Gill (1984) and Yang (personal communication 1995) giving confidence in the equatorial-wave interpretation presented here. An eastward-moving Kelvin wave, symmetric about the equator, emanates from the heating region with a phase speed of about 28° longitude day^{-1}. The westward-moving Rossby solution in the northern hemisphere has a phase speed of about 12° day^{-1}. Without any damping in the system, the flow is still evolving at day 11. However, the central depression of the Rossby solution stabilizes at about 4 hPa and the northern limit of the depression never exceeds about 34°N as seen at day 11.

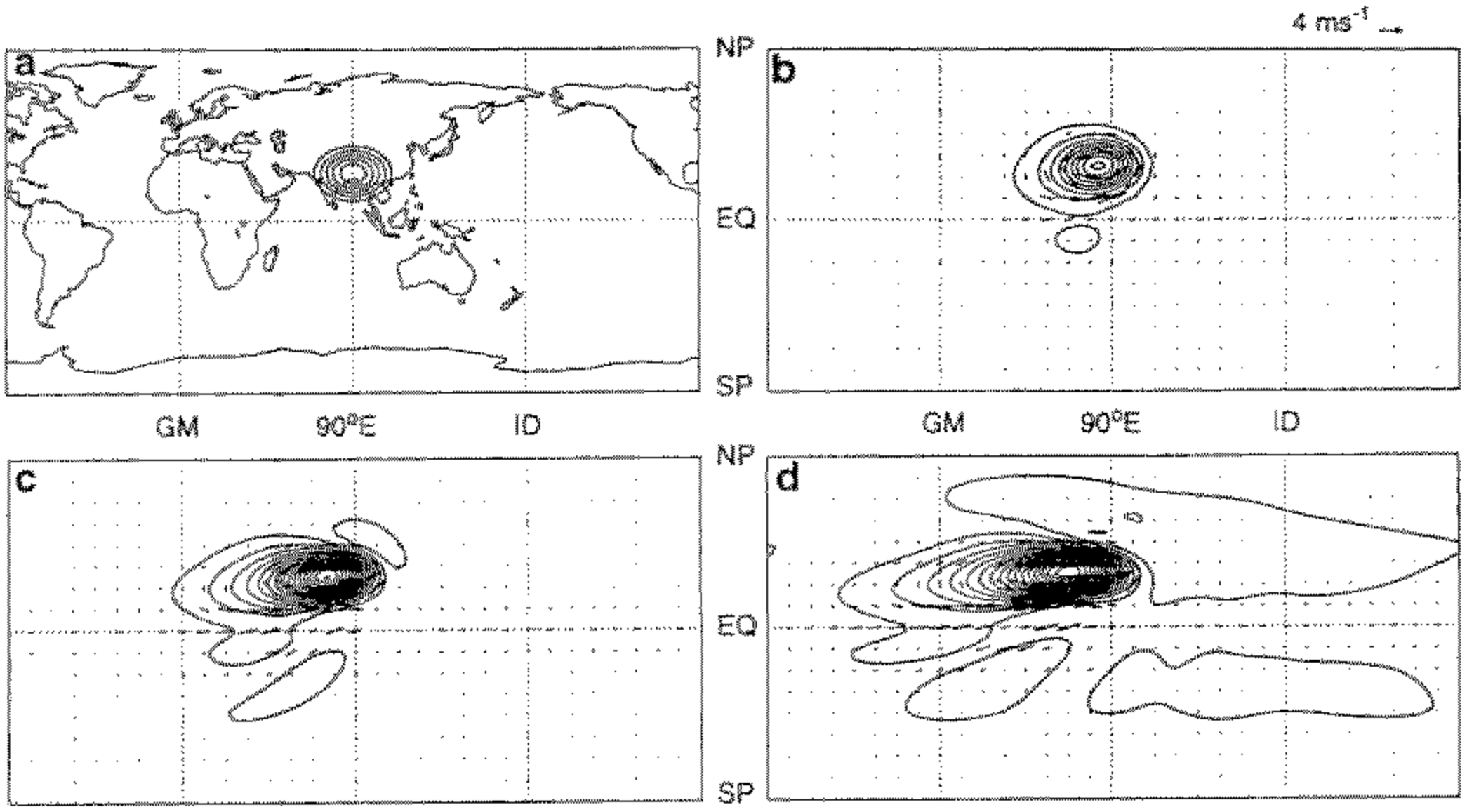

Figure 7. (a) Column-mean diabatic heating centred at 90°E, 25°N. The contour interval is 50 W m^{-2}; the zero contour is not shown. (b), (c) and (d) show the corresponding perturbation surface pressure and 887 hPa horizontal winds for an integration linearized about a resting basic-state at (b) day 3, (c) day 7 and (d) day 11. The contour interval is 1 hPa.

The second integration is exactly the same as the first, but with the heating centre shifted northwards to 25°N, shown in Fig. 7(a). This shift can be thought of as mimicking the monsoon onset. The heating no longer straddles the equator and therefore has a weaker symmetric component at the equator than the 10°N heating field. Figure 7(b, c, d) shows the evolution of the perturbation surface pressure and 887 hPa horizontal winds for days 3, 7, and 11 of this integration. The lack of equatorial symmetry of heating results in a significant weakening of the (symmetric) Kelvin mode, but the northern hemisphere Rossby solution is enhanced strongly, with the central depression stabilizing at about 16 hPa—four times as strong as in the 10°N integration—and extending about 15° latitude further north to nearly 50°N. Interestingly, the wave pattern of the southern hemisphere looks quite similar by day 11 in both of these integrations.

Figure 8(a) shows the pressure and horizontal winds on the 325 K isentropic surface for day 11 of this second integration with heating at 25°N. To the east of the heating region, with no equatorial-wave activity, the thermal structure diminishes rapidly. To the west, the Rossby wave results in a warming of the atmosphere. Since this integration is linearized about a resting basic-state, horizontal advection of temperature must be zero. There is also no Newtonian cooling and so, outside the monsoon-forcing region, the diabatic heating is zero and the thermodynamic-energy equation must take the form

$$\frac{\partial T'}{\partial t} = -\left(\frac{p}{p_0}\right)^{\kappa} \omega' \frac{\partial \bar{\theta}}{\partial p}, \tag{4}$$

where the overbar indicates the basic state and a prime indicates a perturbation from it. The descent, ω', to the west of India, seen in Fig. 8(b), is part of the 'pure' Rossby-wave response to the monsoon heating and, through (4), is consistent with the warm structure over south-west Asia, the Arabian Peninsula, and northern Africa. The warm/descent region continues to expand west during the integration but, once established, the descent over northern Africa remains approximately constant at between 0.4 and 0.5 hPa h^{-1}.

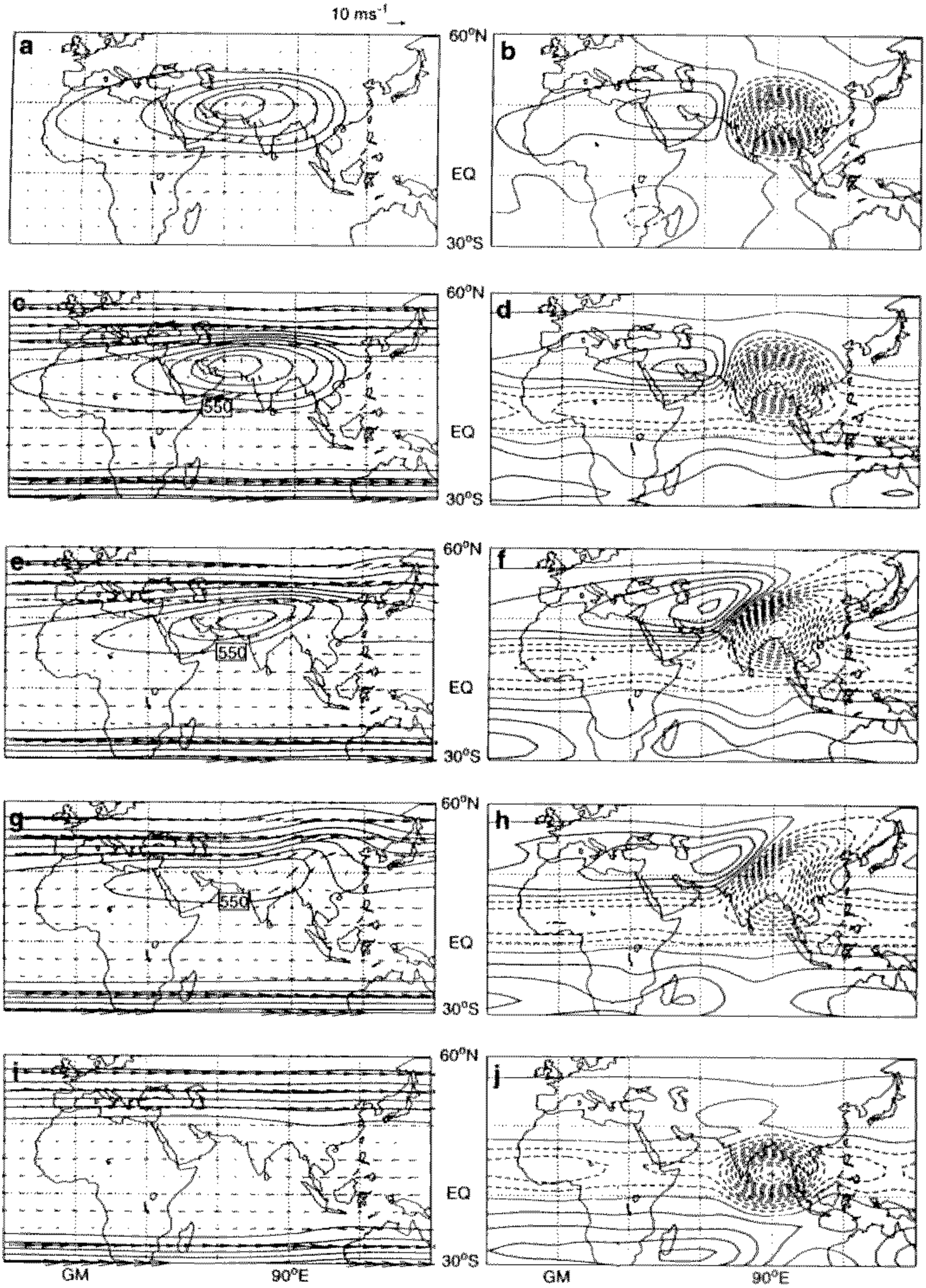

Figure 8. Day 11 of a series of integrations without orography. (a), (c), (e), (g) and (i) pressure and horizontal winds on the 325 K isentropic surface, with contour interval 40 hPa; (b), (d), (f), (h) and (j) vertical velocity at 477 hPa, with contour interval 0.25 hPa hr^{-1}; (a) and (b) integration linearized about a resting basic-state and forced with heating at 90°E, 25°N; (c) and (d) integration linearized about a resting basic-state and forced with heating at 25°N superimposed on the June to August zonal-mean flow; (e) and (f) integration linearized about the zonal-mean basic-state and forced with heating at 25°N; (g) and (h) non-linear integration forced with heating at 25°N; (i) and (j) nonlinear integration forced with heating at 90°E, 10°N.

Consequently, the vertical advection term and $\partial T'/\partial t$ also remain approximately constant at about 0.5 K day^{-1} (at 477 hPa) and the thermal structure continues to intensify.

For comparison with subsequent panels, Fig. 8(c) shows the perturbation thermal structure given by this integration, superimposed on the June to August zonal-mean field. Although the warm region becomes more intense than seen in the observations, Fig. 1(e), (for example the 325 K isentrope dips lower over Pakistan, reaching 710 hPa) the likeness of the structure of the modelled warm region to that seen in the observations is very clear. One can say with some degree of confidence that it is indeed Rossby waves emanating from the monsoon heating region that are responsible for setting up this thermal structure with, in particular, east–west temperature gradients, $\partial T'/\partial x$. Figure 8(d) shows the vertical velocities for this second integration, superimposed on the zonal-mean June to August field. Although the warm structure is too intense, it is clear that the descent is rather weak, too far south and unlocalized when compared with the observations given in Fig. 1(a). Note that the contour interval here is half that used in Fig. 1(a).

The third integration also uses the heating centred at 25°N, but the model is now linearized about the zonal mean of the June to August flow, and the zonal coefficients of the flow are maintained. Linear horizontal advection of temperature is now possible and the extra term, $-(\bar{u}\partial T'/\partial x + v'\partial \bar{T}/\partial y)$, must be included on the right of (4). The horizontal advection of cooler (westerly) air balances both increased adiabatic warming due to increased descent and a reduced temperature tendency, so the integration is now more steady. Typically, the temperature tendency is half the magnitude of the previous integration. Figure 8(e) shows a thermal structure at day 11 which, being weaker, agrees somewhat better in magnitude with the observations than Fig. 8(c), but it is essentially the same Rossby mode as before. The adiabatic descent that balances the horizontal advection term on the southern flank of the mid-latitude westerlies is seen, in Fig. 8(f), to lead to a north-eastward intensification of the descent region of Fig. 8(d). With little mean flow further south, the southern half of the descent region remains very similar to that of the Rossby solution of Fig. 8(d).

The next integration in the series is a full nonlinear integration, with heating centred at 25°N, thermal damping as in the standard integration and with the drag coefficients fixed at the ocean values of the standard integration. The inclusion of the nonlinear terms results in the establishment of a very steady simulated circulation. Indeed, the temperature tendencies over northern Africa and the Mediterranean at 477 hPa are less than 0.05 K day^{-1} by day 18. This contrasts with a magnitude for the local adiabatic cooling resulting from horizontal advection of −0.45 K day^{-1} and for the adiabatic warming resulting from descent of about 0.60 K day^{-1}. The residual −0.10 K day^{-1} is mainly the result of maintenance of the zonal mean circulation in the presence of forced ascent in the monsoon region. The (nearly steady) thermal structure that emerges, Fig. 8(g), agrees well with the observed structure over south-western Asia, the Arabian Peninsula and northern Africa, but is essentially still due to the simple Rossby mode. Figure 8(h) shows the corresponding vertical-velocity field. The descent to the west of the monsoon region is about one fifth of the maximum observed strength shown in Fig. 1(a) and modelled in Fig. 4(b), and is spatially more uniform.

It would appear that remote monsoon heating can induce a general region of descent associated with the linear Gill-type Rossby-wave pattern to its west and that the interaction of the mid-latitude westerlies with the Rossby thermal structure intensifies this descent region north-eastward. However, the monsoon appears to have little or no influence on the observed localization of this descent.

The final integration, shown in Fig. 8(i, j), is exactly the same as the previous non-linear integration, except that the heating field has been moved back to 10°N—perhaps

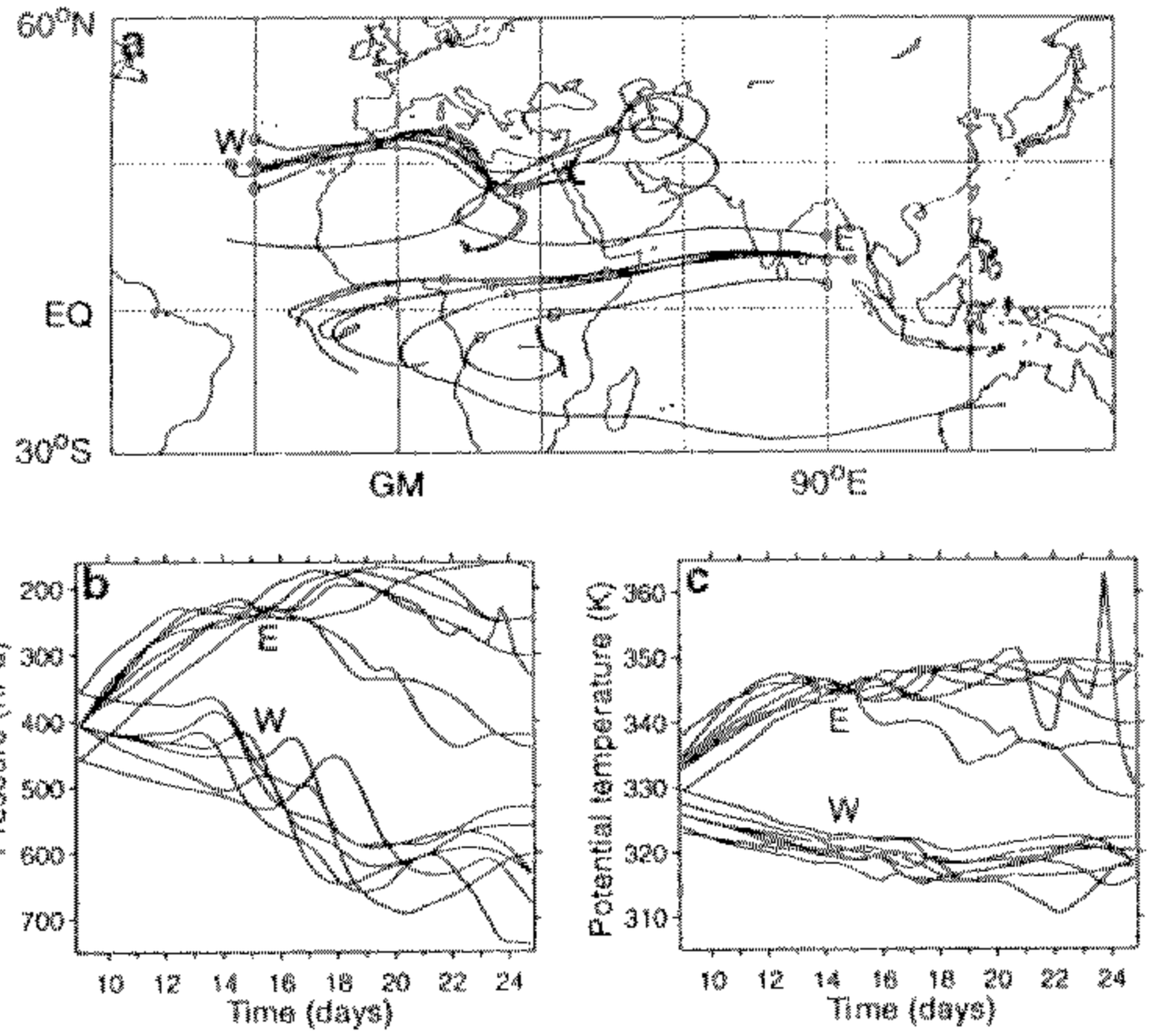

Figure 9. Trajectories for two clusters of seven particles released at day 9 in the standard model integration and advected in three-dimensional space until day 25. Initially, one cluster (termed 'W') is centred on the southern flank of the mid-latitude westerlies around at 30°W, 30°N, $\sigma = 0.4$, and the other (termed 'E') is centred in the tropical easterly flow around 90°E, 10°N, $\sigma = 0.4$. In each cluster, six particles are initially displaced by ±5° of longitude, ±5° of latitude or ±0.05 of σ from a central particle. (a) Horizontal projections of the trajectories—small circles indicate the positions of the particles at days 9 and 17; (b) pressure at each position of each particle; (c) potential temperature at each position of each particle.

representing the latitude of pre-monsoon-onset heating. The four-fold reduced Rossby pressure perturbation seen in the linear integration with heating at 10°N compared with that at 25°N (Fig. 6(d) and Fig. 7(d)) is consistent with the very weak thermal structure seen in Fig. 8(i). The weakening of the Rossby perturbation, and the fact that it does not extend far enough poleward to interact with the mid-latitude westerlies, explains the complete lack of increased descent over south-western Asia, the Arabian Peninsula or northern Africa. Indeed, the descent over these regions is now no stronger than that of the initially-prescribed zonal-mean Hadley circulation. This result suggests that one might expect to see a rather sudden start of the east Mediterranean/Saharan descent, coincident with the northward movement of heating during the monsoon onset.

Although the Asian monsoon appears to play an important role in the descent mechanism, the mechanism does *not* represent a simple overturning circulation often described as a 'Walker-cell'. The idea that air ascends in the Asian monsoon region, flows west in the tropical easterly jet, descends over the Sahara and Arabian deserts and then flows back to the monsoon region is *not* borne out in the results of this study. Figure 9(a) shows the horizontal projection of some 3-dimensional trajectories initiated at about 400 hPa at day 9 in the standard integration with the full orography and heating distribution. Although a limited number of trajectories can be somewhat misleading, the descending air, indicated in Fig. 9(b), would, in agreement with the above series of integrations, appear to have its origin more in the southern flank of the mid-latitude westerlies than in the tropical easterly flow. Figure 9(c) shows that the potential temperature of the westerly air is less than that of the easterly air. Clearly this lateral import of cooler air is essential if the observed

thermodynamic balance is to be achieved. In addition, the potential temperatures of the westerly air particles, Fig. 9(c), cool diabatically (radiatively), accentuating any adiabatic descent, whereas the potential temperature of air in the easterly flow is seen to rise as the air particles cross the Indian subcontinent and the eastern Arabian Sea.

The trajectories of the 'westerly' descending air particles suggest that the anticyclonic centres immediately to the west of the desert descent regions could be important for the localization of descent. The possible descent induced by a Charney-type albedo feedback, and any descent within the desert heat-low circulation, would be accompanied by anticyclonic outflow; there is, however, little in these processes to suggest localization of the desert in the first place. The hypothesis must therefore be that their positioning is influenced by orographic effects.

(*b*) *The effect of orography*

The anticyclonic centres over north-west Africa and south-west Asia, seen from the wind vectors in Fig. 1(e), are both located approximately over high ground—the mountains of northern Algeria, ending at the Haut Atlas at the north-western tip of Africa (0°E, 30°N), and the Zagros mountain chain of Kurdistan and Iran (45°E, 35°N) respectively (Fig. 2(a)). Figure 10 shows the nearly steady mid-tropospheric vertical-velocity field (at day 16) for a non-linear integration with the full mountains, drag and thermal damping of the standard integration, but with no diabatic forcing other than that implied by sustaining the zonal-mean (Hadley) circulation. Although weak, all three northern hemisphere descent-centres identified in Fig. 1(a) are evident—near 20°W, 35°N (over the eastern Atlantic), 20°E, 35°N (near Crete) and 60°E, 45°N (over the Aral Sea). This adiabatic descent can only be thermodynamically balanced in the time-mean flow by horizontal cold advection, associated with anticyclonic circulations induced by the orography.

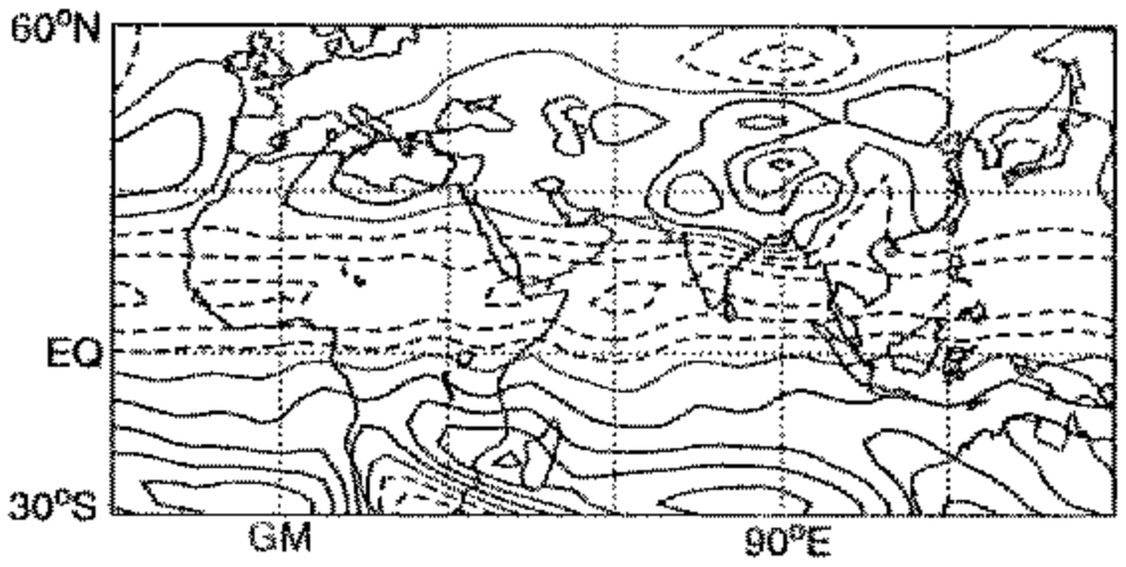

Figure 10. Vertical velocity, ω, at 477 hPa for day 16 of a model integration with full orography but no asymmetric diabatic forcing. The contour interval is 0.25 hPa hr^{-1} and solid contours show descent.

In the light of this result, the southward advection of cold air, seen to be too strong in the standard model integration over the Aral Sea and Arabian Peninsula regions (comparing Figs. 1(e) and 4(a)) would appear to be related to orographic effects. The Zagros mountain range is, in reality, a sharp feature, with many peaks rising to over 4 km. It is possible that the smoothed T31 orography used here does not block the flow sufficiently, allowing low-level westerly flow to pass over the top, as in the linear simulation of Hoskins and Rodwell (1995), and thus exaggerating both the anticyclonic circulation and the southward advection of cold air. Another integration with the Zagros mountains raised by 40%, from about 1 km to 1.4 km, in-line with T31 envelope orography, produced a reduction in this descent of about 20%.

To confirm the importance of local and remote diabatic forcing, and orography, in causing the eastern Sahara/Mediterranean and Kyzylkum descent regions, the results will

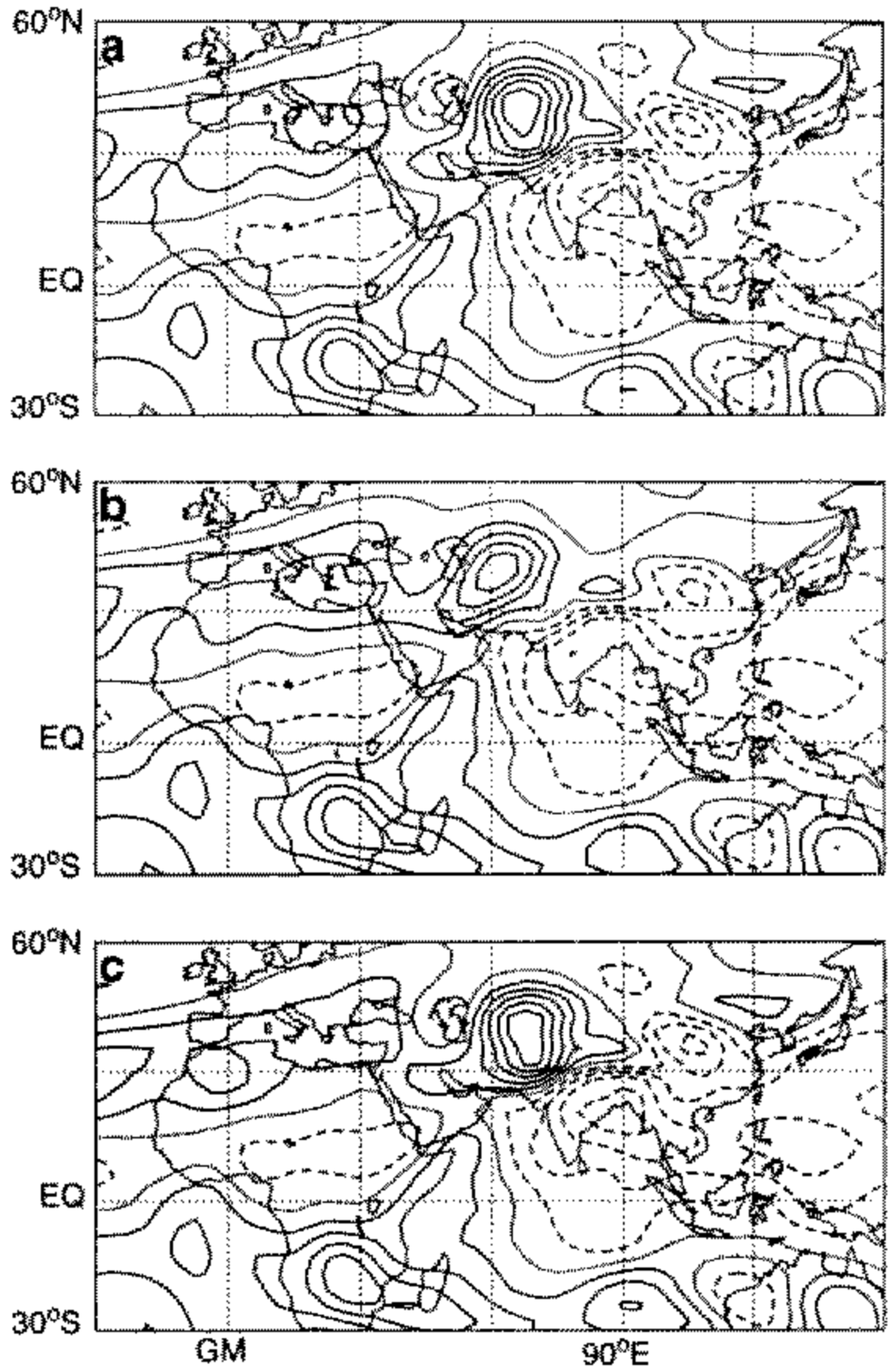

Figure 11. Vertical velocity, ω, at 477 hPa for day 16 of three model integrations. The contour interval is 0.25 hPa hr^{-1}. (a) Full world orography and heating with the exception of no diabatic forcing in the Saharan descent region (0° to 45°E and 15°N to 45°N). (b) As (a) but with the Zagros mountain chain removed (30°E to 60°E and 25°N to 50°N). (c) As (a) but with the Algerian terrain removed (15°W to 20°E and 20°N to 40°N).

now be shown for three experiments which are modifications of the standard integration. In each case the model is nonlinear, with the same drag and thermal damping as in the standard integration. In the first integration, for which the day 16 vertical velocity is shown in Fig. 11(a), the local diabatic forcing in the east Sahara/Mediterranean region (0° to 45°E and 15°N to 45°N) is removed from the heating shown in Fig. 2(b) and Fig. 1(b). A little less than half the time-mean descent observed over the eastern Mediterranean in Fig. 1(a) is still seen. This descent can be considered to be an almost linear sum of the idealized monsoon descent (Fig. 8(h)) and the orographic descent (Fig. 10).

When, in addition to the lack of diabatic cooling in the east Saharan/Mediterranean descent region, the Zagros mountain chain is removed from the model, there is little change in the structure of the north African and Mediterranean descent pattern, shown for day 16 in Fig. 11(b). By contrast, the descent south of the Aral Sea is reduced. This is interesting because the raising of the Zagros and their removal both lead to a reduction in the strength of this descent centre, although for different reasons. The first probably results from increased nonlinear blocking of the flow and the second from reduced linear forcing of the local anticyclonic circulation.

When, instead, the Algerian terrain is removed, the structure of descent over northern Africa and the Mediterranean, shown in Fig. 11(c), is more strongly modified, with more

descent in the Algerian region and less descent over the east Mediterranean region. These results imply that the terrain to the west (upstream) of each descent centre is most important for determining the location of the descent.

(c) *The monsoon–desert mechanism*

The mechanism for desertification proposed here is that the Asian monsoon heating induces a Rossby-wave pattern to its west. Integral with the Rossby pattern is descent and a thermal structure with isentropes sloping down into the monsoon region. Air on the southern flank of the mid-latitude westerlies interacts with the warm structure and, even in the absence of diabatic effects, descends as it glides down the sloping isentropes. The general region of descent forced in this way is localized and enhanced by (up-stream) orography which induces anticyclonic flow and southward advection of cold air to its east. The combined monsoon–mountain effect is *adiabatic* descent, a little under half the 'observed' magnitude, and consequently adiabatic warming, a reduction in the specific humidity of air parcels, a lack of moist convective heating, a lowering of the radiative level with increased radiative cooling in the cloud-free atmosphere and, therefore, *diabatic* descent also. This enhancement is illustrated by the decreasing potential temperatures of the particles in Fig. 9(c). It is speculated that this diabatic enhancement of descent, perhaps aided by albedo effects as suggested by Charney (1975), is responsible for about a doubling of the original adiabatic descent.

In addition, the descent itself may induce further anticyclonic flow below and, therefore, enhanced cold-air advection, explaining an 'observed' slight westward tilting with height of the descent centre.

4. Other evidence for the 'monsoon–desert mechanism'

Practically no rain ever falls during June, July or August at north African locations close to the centre of the 'descent' region. At Alexandria, Egypt, for example, a total of only 3 mm was measured during the 51 year period from 1889 to 1940 (World Weather Records published by the Smithsonian Institute, Washington). The 'monsoon–desert mechanism' suggested here may be so effective that correlations between Asian summer-monsoon intensity and rainfall at the centre of the descent region are (paradoxically) very poor. However, one might expect to see a relation between the Asian monsoon and analysed descent over the eastern Mediterranean region, for example during the rapid onset of the monsoon. Alternatively, one might hope to find correlations for palaeoclimate scenarios with significantly stronger or weaker monsoon circulations.

(a) *The monsoon onset*

Figure 12(a) shows the analysed 477 hPa vertical velocity averaged for the month of May 1994 taken from ECMWF analyses and spectrally smoothed, as outlined earlier. Ascent over southern Asia is confined to its extreme south-east at this time, indicating rather weak monsoon-heating. East Mediterranean descent has a magnitude of about 1.5 to 2 hPa h^{-1}. This descent is about twice as strong as that given by the mountains-only integration, Fig. 10. The difference may be due to the heating over south-east Asia, since Fig. 8 indicates that the precise longitude of the heating is less important than its latitude. However, the difference is consistent with a doubling by local diabatic enhancement, and, perhaps, both factors (and possibly local synoptic events) play some part in the final magnitude of the descent. Figure 12(b) shows a similar picture for June 1994. Heating over south Asia is significantly increased and, in agreement with the monsoon–desert mechanism, the east Mediterranean descent enhances to over 3.5 hPa h^{-1}. Figure 12(c) shows a

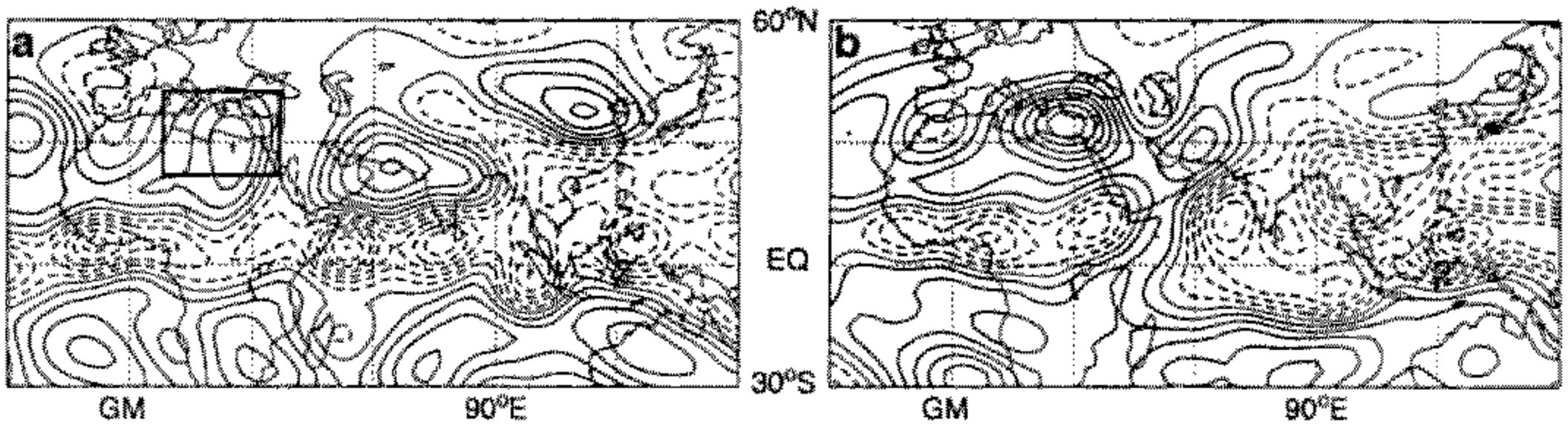

Figure 12. (a) and (b) Vertical velocity ω at 477 hPa, calculated from ECMWF analyses for 1994 and spectrally smoothed; contour interval 0.5 hPa hr^{-1}; (a) May; (b) June. (c) Daily time series and 60-day running mean of ω at 477 hPa at 12 UTC, averaged over the box shown in (a)—(8°E to 37°E and 22°N to 42°N).

daily series of 12 UTC vertical velocity, averaged over a box at 477 hPa over the eastern Sahara/Mediterranean descent region. The wintertime variability over this region, associated with depression activity from the Atlantic, ceases dramatically as the descent intensifies during the onset of the Asian monsoon. One should bear in mind, when viewing this figure, that the zonal-mean descent picture shows completely the opposite, with maximum sub-tropical descent during the *winter* season.

(*b*) *Palaeoclimate studies*

Various geological studies have identified and dated hydrological optimum events over the east Sahara region. These moist events were marked with large, if shallow, lakes and savannah-type vegetation and wildlife.

Szabo *et al.* (1989) found that samples taken from ancient lakes in the Wadi Arid and Wadi Safsaf in southern Egypt, at about 28°E, 22°N, indicated several moist events with ten dates at 45 000 ± 2000 yr ago, and 14 at 141 000 ± 7000 yr ago. One sample yielded an age of 15 000 ± 2000 yr.

Gaven *et al.* (1981), and Gaven (1982) summarized by Lézine and Casanova (1991), studied deposits found in the Wadi Shati, at about 14°E, 27°N, in west central Libya. Isotope analysis indicated the shoreline of a large continental lake whose size peaked at about 2000 km^2 some 133 000 yr before the present day (B.P.). From the volume of the lake, Petit-Maire *et al.* (1991), infer that it must have been fed by rains in both winter and summer. Given the likelihood of ambient descent in the wintertime Hadley cell, summer rains would certainly seem to be vital for the existence of the lake. At present the region receives less than 30 mm of rain annually. The results of Gaven *et al.* (1981) indicated

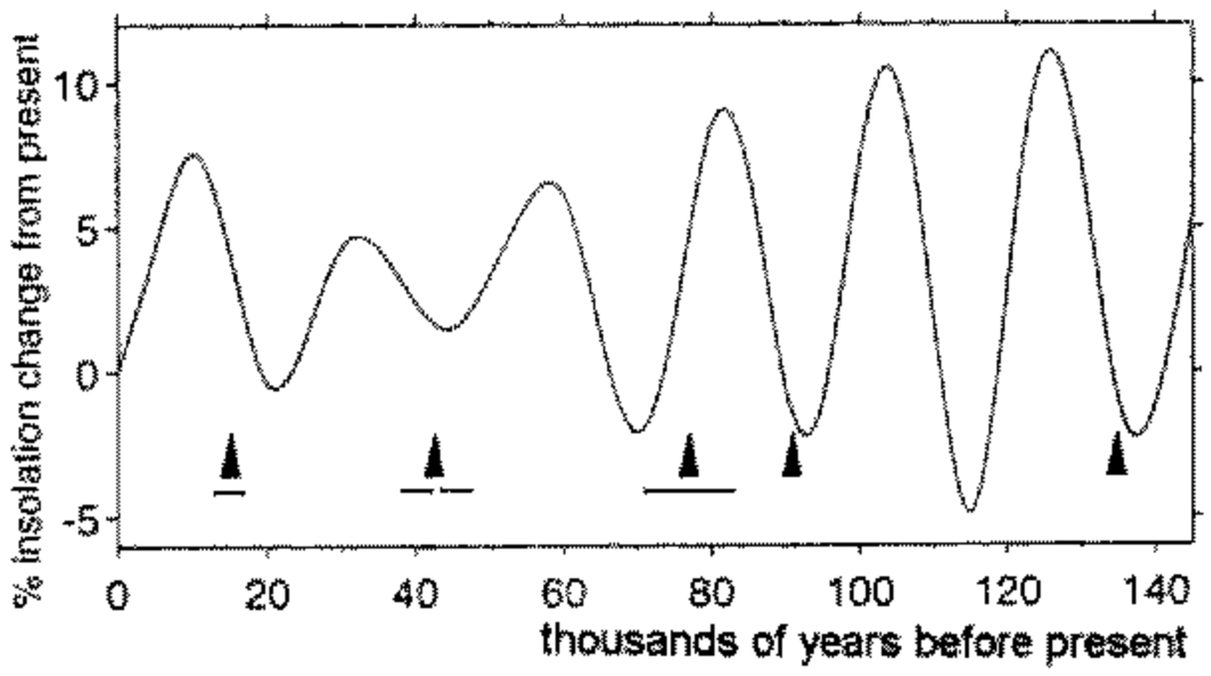

Figure 13. Northern hemisphere insolation in June, July and August, plotted against time, after Prell and Kutzbach (1987). The black arrow heads represent moist events in the eastern Sahara region as summarized by Lézine and Casanova (1991). Error bars are given for the events centred at 15 000, 43 000 and 77 000 yr B.P. See text for a discussion of the possible dating errors for earlier events.

that the lake, which was perhaps 100 km long, oriented east–west, and 10–20 km wide, had fresher water at its eastern end, suggesting freshwater input from the east. Since this lake was located to the west of the descent region identified here, the eastern water-source would be consistent with the shutting-off of the monsoon–desert mechanism. Gaven *et al.* (1981), and Gaven (1982) summarized by Lézine and Casanova (1991), found other moist events, with four dates centred around 91 000 B.P. together with dates of 77 000 (±6000) and 40 000 (±2000) B.P. suggesting more recent but less extensive humid episodes.

Kowalski *et al.* (1989), found moist events at Bir Tarfawi, in the now exceedingly arid eastern Sahara, dated within a 10 000 yr period centred at about 135 000 B.P. Fauna composition from this time suggests a large, rather shallow lake surrounded by savannah, and receiving at least 500 mm of rain annually. Bir Tarfawi is close to Wadi Safsaf and at present receives less than 1 mm rain per annum.

Interestingly, these moist events, shown by black arrow heads in Fig. 13, appear to occur at periods of *minimum* northern hemisphere summertime insolation, which is modulated by changes in the earth's orbit. Error bars are given for the datings of moist events on this figure up to the 77 000 B.P. 'event'. Beyond this time, errors for individual datings can be quite large, e.g. ±15 000 yr around 135 000 B.P. However, many datings have been made for this event and the mean, hydrologically optimum date, as suggested by Lézine and Casanova (1991), is given by the arrows. No results were found to indicate a hydrological *maximum* over the eastern Sahara at the 115 000 B.P. minimum in northern hemisphere summer insolation. However, results of Gaven *et al.* (1981) suggest that the region was still humid at this time.

Changes in the intensity of the Asian summer monsoon have also been strongly linked to the cyclical, Milankovitch, changes in summertime insolation (e.g., Prell and Kutzbach 1987, 1992 and Clemens *et al.* 1991), with increased (decreased) monsoon intensity coinciding with increased (decreased) northern hemisphere summer insolation. Thus these studies would suggest that the Asian monsoon was weak at the minima in the insolation curve in Fig. 13. The near coincidence of the east Sahara moist events, shown by arrows, and these minima is consistent with the mechanism proposed in the present paper.

Kowalski *et al.* (1989) perceived difficulties in relating moist events over the eastern Sahara with the *strong* monsoon events suggested by Prell and Kutzbach (1987). They went on to suggest that the apparent discrepancy was due to imprecision in the dating of the lakes. The present study shows that there could be no discrepancy at all and that moist

events over this eastern Sahara region should, in fact, be correlated with *weak* northern hemisphere summer insolation and a weak Asian monsoon. Clearly, however, there could be inaccuracies in the dating techniques and perhaps the correlation found in the present study should be viewed as indicating the benefits of further geological study in the eastern Sahara and Kyzylkum rather than being conclusive in itself.

Datings of moist events at Chott El Jerid, at about 8°E, 34°N, in southern Tunisia, obtained by Causse *et al.* (1989), are also consistent with the 'monsoon–desert' mechanism, but ancient lake-levels over the western Sahara, summarized by Lézine and Casanova (1991), outside the descent region highlighted here, may *not* show such good agreement with 'Milankovitch–monsoon' forcing. Since the western Sahara is outside the descent region linked to the mechanism in this study, the lack of correlation there supports the local nature of the monsoon/mountain-induced descent.

This local nature of the mechanism is in agreement with the results of coupled GCM–biome model simulation of Claussen (1994) in which the Sahara was initially covered with rainforest. It was shown that trees remained over the western Sahara, consistent with Charney's hypothesis. However, the eastern Sahara returned to desert which is consistent with the monsoon–desert hypothesis proposed here.

5. Discussion

The monsoon–desert mechanism suggested here appears to explain the present-day dry summertime climates of the east Sahara/Mediterranean and Aral Sea regions. Combined with the mean wintertime descent associated with the Hadley circulation, this mechanism can explain the aridity of the east Sahara and Kyzylkum desert regions. It also explains the rapid strengthening of descent over the east Sahara/Mediterranean during the monsoon onset and, indeed, past changes in the climate of this region. If this mechanism is dominant, then, rather than being the initiator of desertification, local radiative cooling should perhaps be viewed in these regions as an enhancing factor, triggered by the monsoon to the east.

The existence of other monsoon-climate regions over the globe may, in a similar way, explain the summertime strengthening of the oceanic subtropical anticyclones and the existence of western continental deserts. This important problem will be explored in a subsequent paper.

Although closer to the Asian monsoon region than the Sahara, the Arabian Desert is less well explained by this mechanism. The Arabian Desert is much further south of the mid-latitude westerlies, and Fig. 1(e) shows that the mean mid-tropospheric flow in June, July and August over the Desert is *away* from the monsoon region, *up* the sloping isentropes. However, mean radiative cooling, Fig. 1(b), offsets this, leaving the weak vertical motion seen in Fig. 1(a).

That the arid and convective regions may be connected has been proposed by others, e.g., Yang *et al.* (1992). However, the link has generally been made via the concept of a closed overturning 'Walker cell' which is not found in our idealized model. If such a closed cell were to exist, then the opposite inference could perhaps be made, viz. that the strength of subsidence over the arid regions influences the intensity of the monsoon. Again, by comparing Fig. 4(b) with Fig. 11(a) over the monsoon region, the present (admittedly simple) model does not support this idea.

The present decline in northern hemisphere summer insolation shown in Fig. 13 would suggest that, on the basis of the hypothesis proposed in this paper, and in the absence of anthropogenic effects, there would be a move towards more moist conditions over the eastern Mediterranean/Sahara and Kyzylkum desert. However, the hypothesis

suggests that any change in Asian summer-monsoon intensity, for whatever reason, for example enhanced greenhouse gases or land-surface changes in southern Asia, would also influence the climate in these desert regions.

Although the timescales are much longer, the present analysis may be of relevance to the question of climate change associated with the uplift of Tibet and the very 'birth' of the Asian monsoon system (see, for example, Kutzbach *et al.* 1989).

Acknowledgements

The possible link between the Asian summer monsoon and descent over North Africa was the subject of many discussions between one of us (BJH) and Dr Prashant Sardeshmukh, and with Professor Robert Pearce. Their contributions are gratefully acknowledged. The authors would also like to thank the Natural Environmental Research Council for its support.

Appendix

Notation used

c_p specific heat of dry air at constant pressure
f Coriolis parameter
H scale height
L horizontal length-scale
N buoyancy frequency
p pressure
p_0 reference pressure of 1000 hPa
Q diabatic heating
T temperature
u speed of wind towards the east
v speed of wind towards the north
$\mathbf{V}$ horizontal wind vector
θ potential temperature
κ R/c_p, the ratio of gas constant to specific heat at constant pressure
σ p/p_0, the vertical coordinate of the model
ω $\mathrm{D}p/\mathrm{D}t$, vertical velocity.

References

Bounoua, L. and Krishnamurti, T. N. 1991 Thermodynamic budget of the five day wave over the Sahara Desert during summer. *Meteorol. Atmos. Phys.*, **47,** 1–25

Causse, C., Coque, R., Fontes, J. C., Gasse, F., Gibert, E., Ben Ouezdou, H. and Zouari, K. 1989 Two high levels of continental waters in the southern Tunisian chotts at about 90 and 150 ka. *Geology*, **17,** 922–925

Charney, J. G. 1975 Dynamics of deserts and drought in the Sahel. *Q. J. R. Meteorol. Soc.*, **101,** 193–202

Claussen, M. 1994 On coupling global biome models with climate models. *Clim. Res.*, **4,** 203–221

Clemens, S., Prell, W., Murray, D., Shimmield, G. and Weedon, G. 1991 Forcing mechanisms of the Indian Ocean monsoon. *Nature*, **353,** 720–725

Ellsaesser, H. W., MacCracken, M. C., Potter, G. L. and Luther, F. M. 1976 An additional model test of positive feedback from high desert albedo. *Q. J. R. Meteorol. Soc.*, **102,** 655–666

Gaven, C. 1982 'Radiochronologie isotopique ionium-uranium'. Pp. 44–54 in Petit-Maire, N., ed., Le Shati, lac Pléistocene du Fezzan (Libye): Marseille, France, Centre National de la Recherche Scientifique

Gaven, C., Hillaire-Marcel, C. and Petit-Maire, N. 1981 A Pléistocene lacustrine episode in south-eastern Libya. *Nature*, **290,** 131–133

Gill, A. E. 1980 Some simple solutions for heat-induced tropical circulation. *Q. J. R. Meteorol. Soc.*, **106,** 447–462

Heckley, W. A. and Gill, A. E. 1984 Some simple analytical solutions to the problem of forced equatorial long waves. *Q. J. R. Meteorol. Soc.*, **110,** 203–217

Hoskins, B. J. 1980 Representation of the earth topography using spherical harmonics. *Mon. Weather Rev.*, **108,** 111–115

1986 Diagnosis of forced and free variability in the atmosphere. Pp. 57–73 in *Atmospheric and Oceanic variability*. Ed. H. Cattle. Royal Meteorological Society, Bracknell

Hoskins, B. J. and Rodwell, M. J. 1995 A model of the Asian Summer Monsoon I: The global scale. *J. Atmos. Sci.*, **52,** 1329–1340

Hoskins, B. J. and Simmons, A. J. 1975 A multi-layer model and the semi-implicit method. *Q. J. R. Meteorol. Soc.*, **101,** 637–655

Hoskins, B. J., Hsu, H. H., James, I. N., Matsutani, M., Sardeshmukh, P. D. and White, G. H. 1989 Diagnostics of the global atmospheric circulation, based on ECMWF analyses 1979–1989. Department of Meteorology, University of Reading. Compiled as part of the U.K. Universities Global Atmospheric Modelling Project, WMO/TD-No.326

Idso, S. B. 1977 A note on some recently proposed mechanisms of genesis of deserts. *Q. J. R. Meteorol. Soc.*, **103,** 369–370

Jin, F.-F. and Hoskins, B. J. 1995 The direct response to tropical heating in a baroclinic atmosphere. *J. Atmos. Sci.*, **52,** 307–319

Kowalski, K., Van Neer, W., Bochenski, Z., Mlynarski, M., Rzebik-Kowalska, B., Szyndlar, Z., Gautier, A., Schild, R., Close, A. E. and Wendorf, F. 1989 A last interglacial fauna from the eastern Sahara. *Quaternary Research*, **32,** 335–341

Kutzbach, J. E., Guetter, P. J., Ruddiman, W. F. and Prell, W. L. 1989 Sensitivity of climate to late Cenozoic uplift in Southern Asia and the American West: Numerical experiments. *J. Geophys. Res.*, **94,** 18393–18407

Lézine, A.-M. and Casanova, J. 1991 Correlated oceanic and continental records demonstrate past climate and hydrology of North Africa (0–140 ka). *Geology*, **19,** 307–310

Matsuno, T. 1966 Quasi-geostrophic motions in the equatorial area. *J. Meteorol. Soc. Japan.*, **44,** 25–43

Petit-Maire, N., Fontugne, M. and Rouland, C. 1991 Atmospheric methane ratio and environmental changes in the Sahara and Sahel during the last 130 kyrs. *Palaeogeogr., Palaeoclimatol., Palaeoecol.*, **86,** 197–204

Prell, W. L. and Kutzbach, J. E. 1987 Monsoon variability over the past 150,000 years. *J. Atmos. Sci.*, **92,** 8411–8425

1992 Sensitivity of the Indian monsoon to forcing parameters and implications for its evolution. *Nature* **360,** 647–651

Rodwell, M. J. and Hoskins, B. J. 1995 A model of the Asian summer monsoon. II: Cross-equatorial flow and PV behaviour. *J. Atmos. Sci.*, **52,** 1341–1356

Ripley, E. A. 1976 Comment on the paper 'Dynamics of deserts and drought in the Sahel', by J. G. Charney. *Q. J. R. Meteorol. Soc.*, **102,** 466–467

Smagorinsky, J. 1953 The dynamical influence of large-scale heat sources and sinks on the quasi-stationary mean motions of the atmosphere. *Q. J. R. Meteorol. Soc.*, **79,** 342–366

Szabo, B. J., McHugh, W. P., Schaber, G. G., Haynes, Jr, C. V. and Breed, C. S. 1989 Uranium-series dated authigenic carbonates and acheulian sites in southern Egypt. *Science*, **243,** 1053–1056

Yang, S., Webster, P. J. and Dong, M. 1992 Longitudinal heating gradient: another possible factor influencing the intensity of the Asian summer monsoon circulation. *Adv. Atmos. Sci.*, **9,** 397–410